

# Impact of electron correlations on two-particle charge response in electron- and hole-doped cuprates

Abhishek Nag,<sup>1,2,\*</sup> Luciano Zinni,<sup>3</sup> Jaewon Choi,<sup>1,4</sup> J. Li,<sup>1,5</sup> Sijia Tu,<sup>6,7</sup> A. C. Walters,<sup>1</sup> S. Agrestini,<sup>1</sup> S. M. Hayden,<sup>8</sup> Matías Bejas,<sup>9</sup> Zefeng Lin,<sup>6,7</sup> H. Yamase,<sup>10</sup> Kui Jin,<sup>6,7</sup> M. García-Fernández,<sup>1</sup> J. Fink,<sup>11,12,†</sup> Andrés Greco,<sup>9,‡</sup> and Ke-Jin Zhou<sup>1,§</sup>

<sup>1</sup>*Diamond Light Source, Harwell Campus, Didcot OX11 0DE, United Kingdom*

<sup>2</sup>*SwissFEL, Paul Scherrer Institute, 5232, Villigen-PSI, Switzerland*

<sup>3</sup>*Facultad de Ciencias Exactas, Ingeniería y Agrimensura (UNR),  
Avenida Pellegrini 250, 2000, Rosario, Argentina*

<sup>4</sup>*Department of Physics, Korea Advanced Institute of Science and Technology (KAIST),  
291 Daehak-ro, Daejeon 34141, Republic of Korea*

<sup>5</sup>*National Synchrotron Light Source II, Brookhaven National Laboratory, Upton, New York 11973, USA*

<sup>6</sup>*Beijing National Laboratory for Condensed Matter Physics,  
Institute of Physics, Chinese Academy of Sciences, Beijing 100190, China*

<sup>7</sup>*University of Chinese Academy of Sciences, Beijing 100049, China*

<sup>8</sup>*H. H. Wills Physics Laboratory, University of Bristol, Bristol BS8 1TL, United Kingdom*

<sup>9</sup>*Facultad de Ciencias Exactas, Ingeniería y Agrimensura and Instituto de Física Rosario (UNR-CONICET),  
Avenida Pellegrini 250, 2000, Rosario, Argentina*

<sup>10</sup>*Research Center for Materials Nanoarchitectonics (MANA),  
National Institute for Materials Science (NIMS), Tsukuba 305-0047, Japan*

<sup>11</sup>*Leibniz Institute for Solid State and Materials Research Dresden, Helmholtzstr. 20, D-01069 Dresden, Germany*

<sup>12</sup>*Institut für Festkörperphysik, Technische Universität Dresden, D-01062 Dresden, Germany*

(Dated: July 23, 2024)

Estimating many-body effects that deviate from an independent particle approach, has long been a key research interest in condensed matter physics. Layered cuprates are prototypical systems, where electron-electron interactions are found to strongly affect the dynamics of single-particle excitations. It is however, still unclear how the electron correlations influence charge excitations, such as plasmons, which have been variously treated with either weak or strong correlation models. In this work, we demonstrate the hybridised nature of collective valence charge fluctuations leading to dispersing acoustic-like plasmons in hole-doped  $\text{La}_{1.84}\text{Sr}_{0.16}\text{CuO}_4$  and electron-doped  $\text{La}_{1.84}\text{Ce}_{0.16}\text{CuO}_4$  using the two-particle probe, resonant inelastic x-ray scattering. We then describe the plasmon dispersions in both systems, within both the weak mean-field Random Phase Approximation (RPA) and strong coupling  $t$ - $J$ - $V$  models. The  $t$ - $J$ - $V$  model, which includes the correlation effects implicitly, accurately describes the plasmon dispersions as resonant excitations outside the single-particle intra-band continuum. In comparison, a quantitative description of the plasmon dispersion in the RPA approach is obtained only upon explicit consideration of re-normalized electronic band parameters. Our comparative analysis shows that electron correlations significantly impact the low-energy plasmon excitations across the cuprate doping phase diagram, even at long wavelengths. Thus, complementary information on the evolution of electron correlations, influenced by the rich electronic phases in condensed matter systems, can be extracted through the study of two-particle charge response.

## I. INTRODUCTION

Interactions among constituent entities lead to emergent phenomena observed across various disciplines, including superconductivity [1, 2], active colloids [3], and neural functions [4]. In condensed matter systems, dynamic behavior of constituent entities is probed using spectroscopic techniques. For instance, in many-electron systems where electron-electron interactions dominate the low-energy physical properties, angle-resolved pho-

toemission (ARPES) or tunneling spectroscopy can assess the strength of ‘electron correlation’. These correlation effects arise from short-range interactions between particles, are seen in the low energy quasi-particle properties. The direct observation of dynamical charge susceptibility, representing the two-particle charge-charge correlation function  $\chi_c''(\mathbf{q}, \omega)$ , in comparison, is possible via spectroscopic techniques such as Resonant Inelastic X-ray Scattering (RIXS) or Electron Energy-Loss Spectroscopy (EELS).

One of the fundamental Bosonic excitations in metallic systems, is plasmon, originating from collective charge density oscillations in the presence of long-range Coulomb interactions [5]. Typically, in isotropic electron systems, the long-wavelength plasmon energy associated with the charge oscillations is finite. In layered-

\* Email: [abhishek.nag@psi.ch](mailto:abhishek.nag@psi.ch)

† Email: [j.fink@ifw-dresden.de](mailto:j.fink@ifw-dresden.de)

‡ Email: [agreco@fceia.unr.edu.ar](mailto:agreco@fceia.unr.edu.ar)

§ Email: [kejin.zhou@diamond.ac.uk](mailto:kejin.zhou@diamond.ac.uk)

3-dimensional (3D) electron systems, the 3D Coulomb interactions are poorly screened due to the confinement of charges to planes separated by dielectric blocks. Thus, although 3D Coulomb interactions tend to forbid gapless plasmons [6], for particular momenta perpendicular to the layers ( $q_z$ ), charge oscillations that are out-of-phase may lead to formation of acoustic plasmons ( $\omega \rightarrow 0$  as  $q \rightarrow 0$ ) along with the gapped (optical) plasmons [7–9].

In layered systems like cuprates, optical plasmons were detected soon after the discovery of the high- $T_C$  superconductivity using Transmission-EELS (T-EELS) [10]. Acoustic-like plasmons in the cuprates, however, have only recently been observed with the development of the RIXS technique [11–16]. Due to the low-energy of acoustic plasmons, their role has been discussed sparsely since the discovery of superconductivity [17–21]. More importantly, the cuprate superconductors, exhibiting anomalous electronic properties such as those observed in the pseudogap and the strange-metal phases [1, 2], are widely studied for correlated electron physics. The observation of long wavelength low-energy quantum fluctuations of charges along with spins [11, 14, 22–24] has, therefore, renewed efforts to develop a unified understanding of electron correlations, Coulomb and exchange interactions aiming towards a microscopic theory [25–28].

Correlation effects in cuprates lead to an enhancement of the quasiparticle electron mass. The mass enhancement factor can be denoted as  $m^*/m$ , where  $m^*$  and  $m$  are the band mass in the presence of interactions and that predicted by tight-binding calculations, respectively [29]. In contrast, a variety of descriptions can be found for the plasmon excitations in the cuprates. The dispersion of the optical plasmons observed using T-EELS has been described within mean-field Random Phase Approximation (RPA) theories without explicitly considering electron correlations [30]. The dispersion of the acoustic-like plasmons observed using RIXS has been described using both free-electron layered models and models incorporating strong electron correlations such as the  $t$ - $J$ - $V$  model [11–14, 27, 28, 31]. The charge carrier doping dependence of plasmon energies could not be explained within a RPA model, leading to the introduction of a scaling factor to the plasmon energies [11, 12]. Recently, the  $t$ - $J$ - $V$  model was employed to explain the low-doping range dependence of plasmons [14, 28]. A similar doping dependence was also discussed in [32], but only for the optical plasma frequency. In the strange metal phase, momentum-independent broad continua observed using Reflection-EELS [33, 34] have been described using holographic theories [35], while a RIXS study has found dispersive excitations in this phase [14]. This multitude of descriptions raises a pertinent question: Do electron correlations that affect the single-particle excitations strongly, have any role to play in the collective charge excitations in cuprates, and what should be the appropriate framework used to describe it?

In this study, we provide a unified perspective on the

importance of electron correlations on the dispersion of the acoustic-like plasmons in electron- and hole-doped cuprates probed by RIXS. We compare equal doping levels ( $\delta = 0.16$ ) of archetypal hole-doped  $\text{La}_{1.84}\text{Sr}_{0.16}\text{CuO}_4$  (LSCO), and electron-doped  $\text{La}_{1.84}\text{Ce}_{0.16}\text{CuO}_4$  (LCCO). The similar lattice parameters of these systems enable investigation of the plasmons in the same momentum phase space. We observe dispersive coherent excitations for both O  $K$ - and Cu  $L_3$ -edge RIXS in both systems. For the equal doping level, we find that plasmon velocity in LSCO is smaller than that of LCCO, consistent with the former’s smaller Fermi velocity derived from bare band electronic dispersion. However, within a free electron model, the plasmon velocities are overestimated when considering the bare Fermi velocities for both systems. We demonstrate that an appropriate fit to experimentally observed plasmon dispersion is possible within a RPA model with the inclusion of a system dependent band renormalization parameter, and without which, unrealistic values of dielectric constants and incoherent excitations are obtained. The acoustic-like plasmons can be accurately described by the  $t$ - $J$ - $V$  model, where bare band parameters provided as input get implicitly renormalized by electron correlations. Our findings reveal that plasmon dispersion in cuprates are affected by electron correlations like the single-particle excitations, and is accounted for by the band renormalization parameter in the RPA model. Thus by comparing plasmon dispersions and bare band electron dispersion parameters, it is possible to assess the role and magnitude of electron correlations in different phases in the cuprates.

## II. RESULTS

### A. Electronic structure of LSCO and LCCO

Hole-doped LSCO and electron-doped LCCO belong to the family of single-layered cuprates, obtained upon doping parent systems  $\text{La}_2\text{CuO}_4$ . They crystallize in distinct structures, the  $\text{K}_2\text{NiF}_4$ -type  $T$  (LSCO) and  $\text{Nd}_2\text{CuO}_4$ -type  $T'$  (LCCO) [37]. In the  $T$  structure, O atoms form octahedral cages around Cu, while apical O atoms are absent in the Cu-O planes in the  $T'$  structure [see Fig. 1(a)], leading to different electronic ground states for the doped systems. A strong Cu-O hybridisation and on-site Coulomb interactions give rise to the Upper Hubbard band (UHB) and the Zhang-Rice singlet (ZRS) band in cuprates, as shown in Fig. 1(b) [36, 38–45]. The electrostatic potential at the Cu sites is raised due to the lack of apical oxygen in LCCO compared to LSCO, resulting in a reduced charge transfer energy ( $\Delta_{\text{CT}}$ ). Hole-doping shifts the chemical potential ( $\mu$ ) to the ZRS, whereas electron-doping shifts it to the bottom of the UHB. The charge carrier dynamics in these systems can therefore be investigated using x-ray spectroscopy by tuning the photon energy to resonant transitions to these bands. The X-ray Absorption Spectra (XAS) of LSCO and LCCO

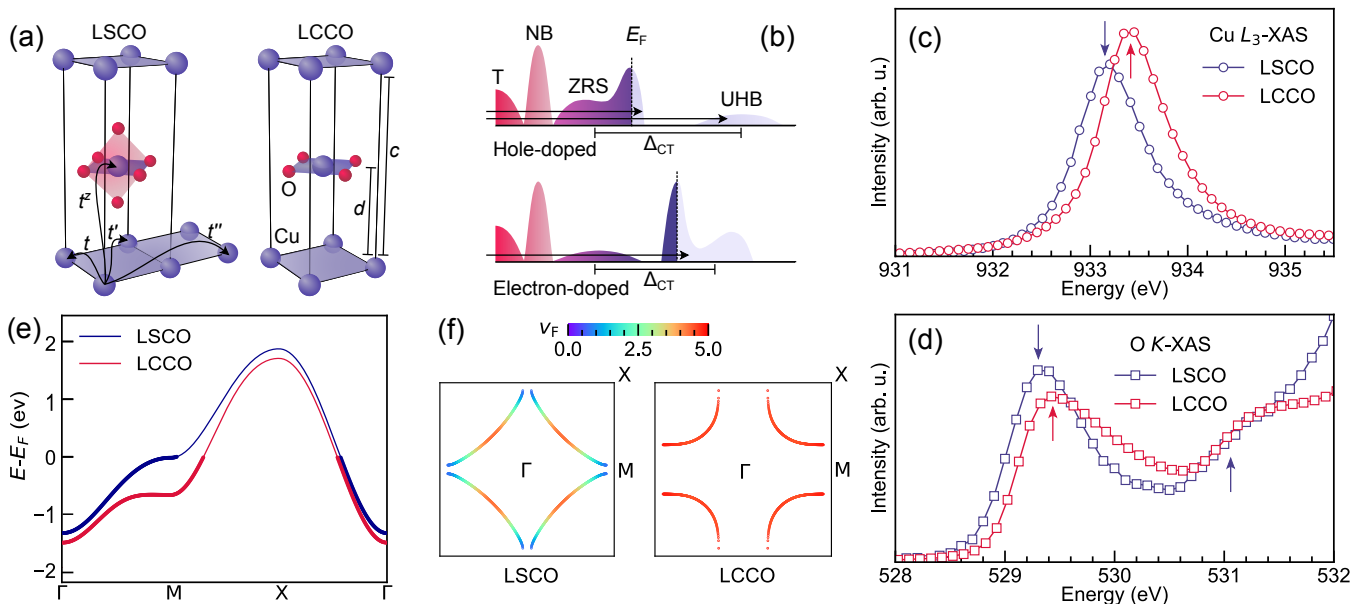


FIG. 1. **Electronic structure of doped cuprates.** (a) Schematic lattice structures of single-layered hole-doped LSCO and electron-doped LCCO showing the Cu-O planes and hopping pathways. Only O atoms around the central Cu atom are shown. (b) Schematic representation of electron transitions within the multi-band structure of hole- and electron-doped cuprates [36]. UHB, ZRS, NB and T represent the Upper Hubbard, Zhang-Rice Singlet, Non-Bonding oxygen, and the Zhang-Rice Triplet bands, respectively. (c) Cu  $L_3$ -edge XAS of LSCO and LCCO. (d) O  $K$ -edge XAS of LSCO and LCCO ( $\delta = 0.16$ ). Arrows mark the photon energies used to probe the plasmons. (e) One-band tight-binding electron dispersion of LSCO and LCCO (see Eq. 4 in Sec. IV B). (f) Fermi velocity distribution in LSCO and LCCO.

( $\delta = 0.16$ ), obtained at the Cu  $L_3$ - and O  $K$ -edge, respectively, are shown in Fig. 1(c) and (d). The Cu  $L_3$ -edge XAS peak corresponds to transition to the UHB in both systems. In LSCO, the first peak in O  $K$ -edge XAS corresponds to the hole-states, with the transition to the UHB occurring 1.5 eV higher [43, 45, 46]. In LCCO, the first peak in the O  $K$ -edge XAS is the transition to the UHB, lowered in energy due to the reduced  $\Delta_{CT}$  and chemical shift of the O  $1s$  level, consistent with observations in electron-doped  $\text{Nd}_{2-x}\text{Ce}_x\text{CuO}_4$  (NCCO) [45, 46].

## B. RIXS

Fig. 2(a-e) show the RIXS energy-momentum maps collected at Cu  $L_3$ - and O  $K$ -edge on LSCO and LCCO ( $\delta = 0.16$ ) [incident photon energies corresponding to the arrows in Fig. 1(c) and (d)] along the Cu-O in-plane direction  $h$ , with  $k = 0.0$  and  $l = 1.0$ . We denote momentum transfers along  $h$ ,  $k$ , and  $l$  directions in reciprocal lattice units, where  $\mathbf{q} = (ha^*, kb^*, lc^*)$  ( $a^* = 2\pi/a$ ,  $b^* = 2\pi/b$ ,  $c^* = 2\pi/c$ , and  $a = b$  and  $c$  are the in-plane and out-of-plane lattice parameters, respectively, see Tab. I). The plasmons are observed as well-defined peaks for both Cu  $L_3$ - and O  $K$ -edge transitions to UHB for LCCO. For LSCO, the plasmons are prominent at O  $K$ -edge when excited at either the ZRS energy or at the UHB, consistent with a previous report [13].

Surprisingly, our earlier investigation on LSCO and  $\text{Bi}_2\text{Sr}_{1.6}\text{La}_{0.4}\text{CuO}_{6+\Delta}$  [31], along with studies on other hole-doped cuprates [22, 47, 48], did not reveal presence of plasmons at Cu  $L_3$ -edge. However, in this study, we conducted measurements at  $l = 1.0$  on LSCO, where the plasmon spectral weight is expected to be the strongest [28]. We can identify faint spectral weight at the Cu  $L_3$ -edge [Fig. 2(a) and (f)], resembling the plasmon dispersion at the O  $K$ -edge. Notably, the observation of plasmons at both the hole-state and UHB of O  $K$ -edge is insufficient to imply a hybridised scenario for the doped charges as mentioned in an earlier study [13]. The presence of plasmons at the Cu  $L_3$ -edge, albeit extremely weak, validates their hybridised nature in the hole-doped cuprate.

Representative fits to the plasmon excitations in the RIXS line profiles, along with other components for the two systems, are shown in Fig. 2(g-j), as described in Sec. IV A. The plasmon energies and widths extracted from the fits are presented in Fig. 3. It is clear from the similarity of plasmon energies and the widths, that we probe the same charge oscillations at Cu  $L_3$  and O  $K$ -edges for LCCO, and the hole-state and UHB peak at O  $K$ -edges for LSCO [Fig. 3(a)]. The plasmons exhibit a nearly linear dispersion for small  $h$ -values; however, since we cannot resolve the plasmon peaks below  $h = 0.02$ , and a gap may exist at  $h, k = 0.0$  due to inter-layer hopping ( $t_z$ ) [27, 49], we describe these excitations to be acoustic-

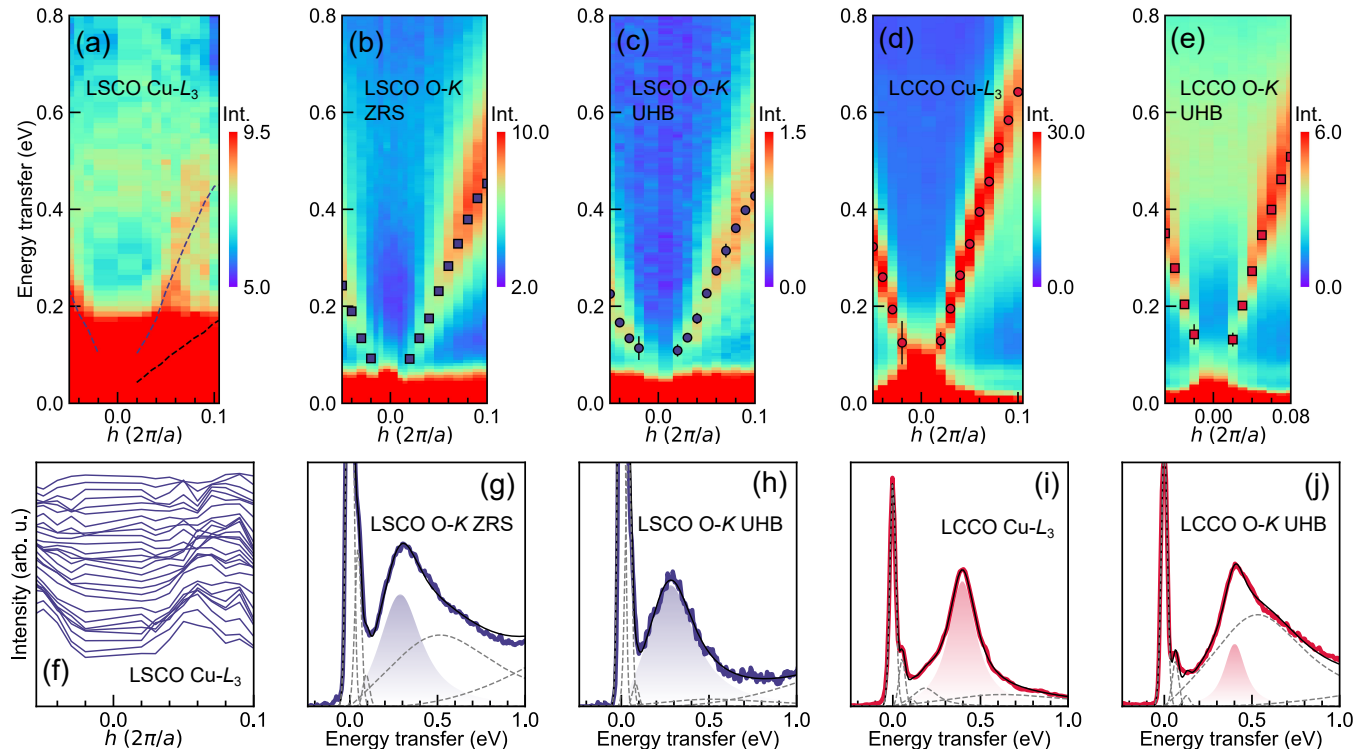


FIG. 2. **Energy-momentum distribution of plasmons in LSCO and LCCO** ( $\delta = 0.16$ ). RIXS intensity maps with incident photon energy at (a) Cu  $L_3$ -edge, (b) O  $K$ -edge ZRS and (c) O  $K$ -edge UHB, respectively, for LSCO. RIXS intensity maps with incident photon energy at (d) Cu  $L_3$ -edge and (e) O  $K$ -edge UHB, respectively, for LCCO. For all the data,  $k = 0.0$  and  $l = 1.0$ . The color scales indicate scattered intensities in arb. u. The markers denote the extracted plasmon energies. In panel (a), the blue dashed line is the plasmon dispersion extracted from panel (b), and the black dashed line is the extended paramagnon dispersion from Ref. [24] for LSCO. Panel (f) shows the momentum distribution curves for energy transfer between 0.225-0.515 eV for Cu  $L_3$ -edge RIXS on LSCO showing the plasmons. (g)-(j) RIXS line spectra from panels (b)-(e) at  $h = 0.06$ . The dashed lines are elastic, lattice, magnetic and background components as described in Sec. IV A. The shaded distributions are the fitted plasmon peaks which can be compared with the calculated charge susceptibility line profiles in Fig. 4(f-h).

like. Note that an upper limit of  $t_z$  was estimated to be 7 meV for LSCO and LCCO [31, 49], which is negligibly small to influence the analysis presented in this work. We observe that the plasmon energies for LSCO are smaller than LCCO for the same doping level and at same  $h, k = 0.0, l = 1.0$  values. The plasmons in LSCO are more damped than LCCO [Fig. 3(b)]. Nevertheless, the damping factor  $\gamma/\omega < 1$ , where  $\gamma$  and  $\omega_0$  represent the plasmon width (damping  $\sim$  inverse lifetime) and plasmon pole energy, respectively, signifying the coherence of the excitations.

### C. Effective masses and Fermi velocities in LSCO and LCCO

For the same amount of electron/hole doping, the plasmon energies extracted from RIXS for LSCO are smaller than in LCCO [Fig. 3(a)], with plasmon velocities  $v_p^{\text{LSCO}} = 2.79 \pm 0.04 \text{ eV\AA}$  and  $v_p^{\text{LCCO}} = 4.20 \pm 0.01 \text{ eV\AA}$ . We first attempt to qualitatively describe the observed plasmon dispersion using the homogenous free-electron

layered model (see Eq. 12) [7]. Note that this free-electron model is in the hydrodynamic limit and also does not consider interlayer hopping, and as such is not strictly applicable to the cuprates. Although less rigorous compared to many-body models, its simple analytic form allows a rudimentary association of the electronic band parameters to the acoustic plasmon dispersion and the optical plasmon frequency  $\Omega_p$ . The acoustic plasmon velocity  $v_p$  at  $l = 1.0$  and small in-plane momentum can be related to the average Fermi velocity  $\langle v_F \rangle$  using Eq. 12 by,

$$v_p = \sqrt{\frac{\langle v_F \rangle^2}{2} + \frac{d^2 \Omega_p^2}{4}}, \quad (1)$$

where,  $d$  is the distance between planes. Assuming that the plasmons are unaffected by electron correlations, we can then use experimentally reported  $\Omega_p$  (see Tab. I) and bare  $\langle v_F \rangle$  extracted from electron band dispersion to approximately estimate the  $v_p$ . We take tight-binding derived bare parameters for LSCO and NCCO (for LCCO) from Ref. [51] (see Eq. 4 in Sec. IV B), and compute the chemical potential  $\mu$  for doping  $\delta = 0.16$ . In Fig. 1(e) we



TABLE I. Parameters for LSCO and LCCO. In-plane lattice constant:  $a$ . Distance between the Cu-O layers:  $d = c/2$ . Doping concentration:  $\delta$ . Superconducting transition temperature:  $T_c$ . Average bare Fermi velocity:  $\langle v_F \rangle^{\text{bare}}$ . Optical plasmon energy:  $\Omega_p$ . Plasmon velocity obtained using  $\langle v_F \rangle^{\text{bare}}$  in Eq. 1:  $v_p^{\text{bare}}$ . Experimental plasmon velocity:  $v_p^{\text{RIXS}}$ . Mass enhancement factor obtained using  $v_p^{\text{RIXS}}$  and renormalized  $\langle v_F \rangle$  in Eq. 1:  $m^*/m$ .

	$a$ (Å)	$d = c/2$ (Å)	$\delta$	$T_c$ (K)	$\langle v_F \rangle^{\text{bare}}$ (eVÅ)	$\Omega_p$ (eV)	$v_p^{\text{bare}}$ (eVÅ)	$v_p^{\text{RIXS}}$ (eVÅ)	$m^*/m$
LSCO	3.77	6.55	0.16	38	2.86	0.8 [50]	3.31	2.79	2.0
LCCO	4.01	6.23	0.16	7.87	4.58	1.2 [12]	4.94	4.20	1.7

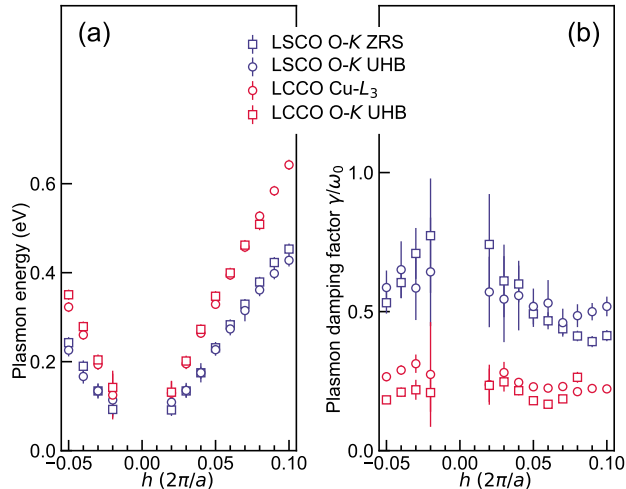


FIG. 3. **Plasmon energies and lifetimes in LSCO and LCCO** ( $\delta = 0.16$ ). (a) Plasmon energies extracted from fits to RIXS spectra at O  $K$ -edge ZRS and O  $K$ -edge UHB for LSCO and Cu  $L_3$ -edge and O  $K$ -edge UHB for LCCO. (b) Plasmon damping and damping factor ( $\gamma/\omega_0$ ) extracted from the same fits.

show the bare band dispersion for LSCO and LCCO. The  $3d$  band is close to half-filling for hole-doped cuprates while for electron-doped cuprates the band-filling is about 70%. Due to the proximity to the van Hove filling, this results in a smaller average bare Fermi velocity  $\langle v_F \rangle^{\text{LSCO,bare}} = 2.86$  eVÅ than  $\langle v_F \rangle^{\text{LCCO,bare}} = 4.58$  eVÅ [shown in Fig. 1(f)]. Using these values in Eq. 1, we obtain  $v_p^{\text{LSCO,bare}} = 3.31$  eVÅ and  $v_p^{\text{LCCO,bare}} = 4.94$  eVÅ. It is expected that the plasmon velocities in hole-doped cuprates are smaller than the electron-doped cuprates with similar  $d$ , due to smaller  $\langle v_F \rangle$ , however, as shown in Fig. 4(a), the Fetter model with the bare band parameters overestimates the plasmon velocities by 17% comparing to the values extracted from RIXS (see Tab. I). Conversely, if we use Eq. 1 and  $v_p$ 's extracted from RIXS, we obtain  $\langle v_F \rangle^{\text{LSCO}} = 1.36$  eVÅ and  $\langle v_F \rangle^{\text{LCCO}} = 2.71$  eVÅ. These values are nearly 50% of the bare band estimates for both systems. Therefore, to explain the experimental results in this approximate model, one needs to use renormalized band dispersions which amount to mass enhancement of  $m^*/m = 2.0$  and  $m^*/m = 1.7$  for LSCO and LCCO, respectively.

#### D. Random Phase Approximation

Next, we consider the explicit description of the plasmons within a RPA framework with long-range Coulomb interaction for a layered lattice system (see Sec. IV B for details of the implementation). Note that we have ensured that the calculations are consistent with the experimentally reported values of  $\Omega_p$  for both systems. In Fig. 4(b) and (c), we show the plasmon dispersion extracted from plasmon peaks in  $\chi''_{\text{RPA}}(\mathbf{q}, \omega)$  calculated with bare and renormalized band parameters so that  $m^*/m = 1.0$  and  $m^*/m = 2.0$  for LSCO, and  $m^*/m = 1.0$  and  $m^*/m = 1.7$  for LCCO. Also plotted, are the upper boundaries of the electron-hole continua for the respective  $m^*/m$  values. For both systems, in the long-wavelength limit, the agreement with the experimental results appears to be slightly better for  $m^*/m = 1.0$ , while above  $h = 0.06$ , the calculated results for  $m^*/m > 1.0$  have smaller deviations from experiments. The momentum dependent deviation from the experimental plasmon energies for LSCO is highlighted in panel (e), showing the better agreement with  $m^*/m > 1.0$  for larger momenta and energies. It should also be noted from panels (b) and (c) that, for  $m^*/m = 1.0$ , the plasmons are within the continuum boundary, while for  $m^*/m > 1.0$ , they are clearly above the continuum. Panels (f) and (g) show the  $\chi''_{\text{RPA}}(\mathbf{q}, \omega)$  and the real part of the dielectric function  $\Re\epsilon(\omega)$  for  $h = 0.06$ , which undergoes a sign change only for  $m^*/m > 1.0$ . This signifies that true plasmon resonances which are long-lived are obtained only for  $m^*/m > 1.0$ . We can compare this observation to the experimentally extracted ratio  $\gamma/\omega_0$  [see Fig. 3(b)]. The  $\gamma/\omega_0$  values are less than 1, which mean that experimentally we observe the plasmons as coherently propagating excitations. Additionally, the ratio of in-plane to out-of-plane dielectric constants obtained from the RPA analysis (see Tab. II in Sec. IV B), for  $m^*/m > 1.0$  is 1.22 for LSCO and 1.32 for LCCO, while for  $m^*/m = 1.0$  the respective ratios are unrealistic ( $\ll 1$ ): 1/6 and 1/4. Thus, the layered lattice RPA model also suggests the use of renormalized band parameters for both systems for describing the plasmons.

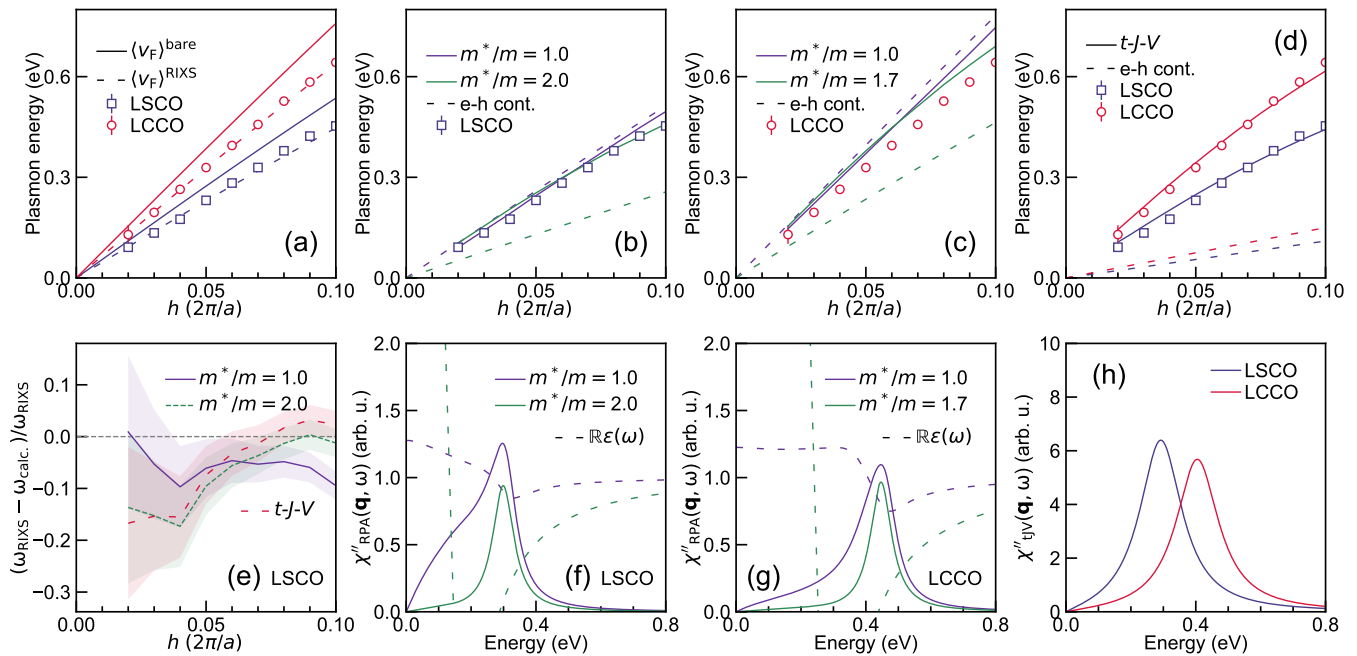


FIG. 4. **Comparison of plasmons to weak- and strong-electron coupling models.** (a) Plasmon energies from RIXS for LSCO and LCCO (markers). Lines are plasmon energies calculated using the free-electron Fetter model (Eq. 1) and different  $\langle v_F \rangle$ s for LSCO and LCCO. (b) Plasmon energies from RIXS for LSCO (markers). Lines are plasmon energies (continuous) and upper boundaries of electron-hole continua (dashed) calculated using the weak-coupling RPA model with different  $m^*/m$  values for LSCO. (c) Same as in (b) for LCCO. (d) Plasmon energies from RIXS for LSCO and LCCO (markers). Lines are plasmon energies (continuous) and upper boundaries of electron-hole continua (dashed) calculated using the strong-coupling  $t$ - $J$ - $V$  model and bare band parameters for LSCO and LCCO. (e) Momentum dependent deviation of the plasmon energies calculated using the RPA and the  $t$ - $J$ - $V$  models from experiments on LSCO. The shaded areas represent the propagated fitting errors from RIXS spectra. (f) Charge susceptibilities (continuous lines) and real part of the dielectric functions (dashed lines) at  $h = 0.06$  obtained from the RPA model with different  $m^*/m$  values for LSCO. (g) Same as in (f) for LCCO. (h) Charge susceptibilities obtained from the  $t$ - $J$ - $V$  model at  $h = 0.06$  for LSCO and LCCO. The charge susceptibility line profiles in panels (f-h) can be compared to corresponding plasmon peaks in RIXS [Fig. 2(g-j)].

### E. $t$ - $J$ - $V$ model

In this section, we model the observed plasmon dispersion with the  $t$ - $J$ - $V$  model with long-range Coulomb interaction for a layered lattice system, where our inputs are the bare band parameters (see Sec. IV B for details of the implementation). Once again, we have ensured that the calculations are consistent with the experimentally reported values of  $\Omega_p$  for both systems. In Fig. 4(d), we show that there is a good agreement between the plasmon dispersions obtained experimentally and those extracted from plasmon peaks in the calculated  $\chi''_{tJV}(\mathbf{q}, \omega)$ . The plasmons appear as well-defined peaks [Fig. 4(h)] and above the electron-hole continuum. This is because the bare band parameters are implicitly renormalized by electron correlations within the theory. To have an estimation of the band renormalization one can see Eq. 25 in Sec. IV B 4, which gives  $m^*/m$  of around 4.5 for both systems. Also, the ratio of the in-plane to out-of-plane dielectric constants obtained from the  $t$ - $J$ - $V$  analysis is found to be 1.35 for LSCO and 1.46 for LCCO (see Tab. II in Sec. IV B). Thus, the strongly correlated

electron model also describes the plasmons appropriately, without explicitly invoking renormalized band parameters.

## III. DISCUSSION

### A. Plasmon dispersion and correlations

Despite the large diversity in material dependent properties, the correlated electron nature of cuprates is widely acknowledged. While the single-particle electron excitations in cuprates clearly show the effects of correlations like mass enhancement and incoherence, charge excitation like the plasmons, have been described using theories ranging from free-electron, weak to strong-coupling. The optical plasmon energy  $\Omega_p$  for zero momentum in the mean-field RPA of homogenous layered electron systems is proportional to  $\sqrt{1/m^*}$  [52, 53]. The optical plasmon dispersion up to second order in  $q$  in this model is  $\Omega_p + Aq^2$ , where  $A$  is a dispersion coefficient dependent on  $m^*$ . Even so, the optical plasmon dispersion observed in

$\text{Bi}_2\text{Sr}_2\text{CaCu}_2\text{O}_8$  using T-EELS could be described using the bare band parameters [52, 53]. Notably, in  $\text{Sr}_2\text{RuO}_4$ , a system for which ARPES estimated  $m^*/m = 4$ , acoustic plasmons observed using EELS have been modeled using bare band parameters [54, 55].

We observe that the plasmon velocity of LSCO is approximately 1.5 times smaller than LSCO for a doping  $\delta = 0.16$ . Since the plasmons are collective excitations involving electrons near the Fermi surface, one can qualitatively explain this observation by considering the 1.5 times smaller  $\langle v_F \rangle$  in the hole-doped cuprate. However, when using the  $\langle v_F \rangle$ s derived from bare bands, the plasmon energies are overestimated for both systems in the free electron model. Therefore, it seems necessary to consider the effects of correlation for a quantitative comparison. Within the RPA approach, the agreement of the dispersion with  $m^*/m = 1$  worsens as  $q$  increases, while it improves for  $m^*/m > 1$ . Although it may seem that the effects of correlation may be fully relaxed in the long-wavelength limit, using the  $m^*/m = 1$  band parameters result in plasmons appearing within the electron-hole continuum and unreasonable dielectric constant values for either system in our model. The value of the mass enhancement factor  $m^*/m = 2.0$  for LSCO is numerically equal to that measured using ARPES at the nodal point [56]. However, this match should not be overemphasised, given that the result from the plasmons represents an average effect over the entire Brillouin Zone (BZ), which means including the anti-nodal region near the saddle point  $(\pi, 0)$  with a low  $v_F$ , and the nodal region near  $(\pi, \pi)/2$ . Also, smaller  $m^*/m$  values are observed in the RPA models for LCCO than LSCO. Although weaker correlations are expected in electron-doped than in hole-doped cuprates [37, 38, 57–62], it should be noted that the  $m^*/m$  values obtained for LCCO, are using the band parameters of NCCO in the calculations due to unavailability of the same for LCCO.

It can be seen from Fig. 4(e) that the deviation from the experiments in the  $t$ - $J$ - $V$  model, in which the correlation effects are implicit, is similar to that obtained from RPA for  $m^*/m > 1$  [smaller (larger) difference at high (low)  $q$ ]. In the  $t$ - $J$ - $V$  model, the bare band parameters get renormalized by the doping  $\delta$  and  $J$ , and additionally the charge response contains fluctuations of the constraint that prohibits double occupancy at a given site. To compare with the RPA model, we use the renormalized band parameters obtained from  $t$ - $J$ - $V$  in the RPA and plot the calculated plasmon dispersions for LSCO and LCCO in Fig. 5. We observe that in the long-wavelength region, the  $t$ - $J$ - $V$  and RPA plasmon dispersions coincide. However, at short-wavelengths, the RPA plasmon dispersions deviate from the  $t$ - $J$ - $V$ . In Fig. 5, we also plot plasmon dispersions obtained from the  $t$ - $J$ - $V$  excluding some bosonic self-energy components (see Sec. IV B 4). Exclusion of these components from  $t$ - $J$ - $V$  results in a mathematically identical form of charge susceptibility to RPA and hence identical plasmon dispersions are obtained for the two models. Thus, it is evident

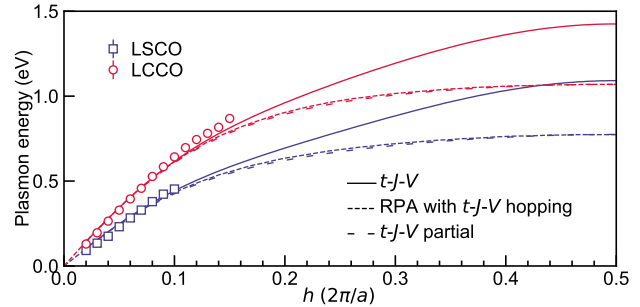


FIG. 5. **Momentum dependence of correlation effects on plasmons.** Plasmon energies from RIXS for LSCO and LCCO (markers). Continuous lines are plasmon energies calculated using the full  $t$ - $J$ - $V$  model. Dense dashed lines are plasmon energies calculated using the RPA model with renormalized band parameters obtained from the  $t$ - $J$ - $V$  model. The match between the two models at long wavelengths suggest that RPA with the renormalized band mass formalism accounts for the effects of electron correlations in this region of momentum space. Locally strong correlation effects stemming from double occupancy prohibition that are absent in RPA, lead to deviations only at large momenta. Sparse dashed lines are plasmon energies calculated using a partial  $t$ - $J$ - $V$  model (see Sec. IV B 4). The overlapping dispersions obtained from the RPA and the partial  $t$ - $J$ - $V$  model show that despite the apparent complication of the  $t$ - $J$ - $V$  formalism with respect to RPA, it has a "hidden" RPA structure including the effects of the electronic correlations.

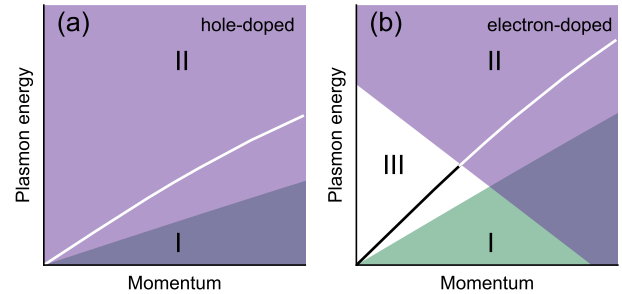


FIG. 6. **Broadening of plasmons due to a decay into single-particle transitions.** The electron-hole continuum due to intra-band transitions (I). The continuum due to umklapp scattering related to inter-band transitions (II). Energy-momentum pocket devoid of continuum in electron-doped systems (III). White lines: Plasmon damping caused by decay into the continuum from single-particle transitions. (a) LSCO, close to half-filled conduction band. (b) LCCO with additional filling of the conduction band, causing a pocket in the continuum of the inter-band continuum.

that the use of renormalized band parameters in RPA accounts for electron correlations through the enhanced band mass at long wavelengths, while the locally strong correlation effects stemming from double occupancy prohibition that are absent in RPA, lead to deviations only at large momenta.

## B. Plasmon Width

In a free-electron model there is no momentum phase space for the decay of an acoustic plasmon into intra-band electron-hole excitations (Landau damping), if the plasmon is above the continuum (region I in Fig. 6). Moreover, in the long-wavelength region, the plasmon should be undamped because the restoring forces of the plasmon are determined by surface charges. Thus, the plasmon width had been a puzzle for long time. Finally, it was theoretically proposed [63] that plasmon width appears through a decay into the continuum formed due to inter-band excitations (region II in Fig. 6). The latter originate from *umklapp* processes due to the square of the Fourier transform of the pseudo-potential of the ions in neighbouring BZs. Experimentally, this was supported by EELS on alkali metals, where the plasmon width was found to be proportional to the square of the pseudo-potential [64, 65]. From the  $\gamma/\omega_0 < 1$  values extracted from RIXS [Fig. 3(b)], we can see that the damping of acoustic plasmons in LSCO is twice as large than LCCO. In the case of a half filled band such as in LSCO and a  $k_F$  equal to half of the BZ, the inter-band continuum extends to  $(q, \omega = 0)$ . Thus, the acoustic plasmons are damped additionally regardless of the intra-band continuum. Upon changing the band filling, a pocket appears in the inter-band continuum in the low-energy low-momentum region (region III in Fig. 6(b)). In this case (e.g. in LCCO), the acoustic plasmon will be less damped.

Additionally, using dynamical mean field theory in the Hubbard model, in Ref. [66], plasmons were obtained if one-particle self-energy effects and vertex corrections due to correlations are treated properly. The inclusion of self-energy effects leads to a broadening of the plasmons (in addition to mass enhancement), and an energy dependence of the mass enhancement can not be ruled out [67–69]. One-particle self-energy effects can easily be expected from the interaction between carriers and the rich variety of low-energy charge excitations in the scale of  $J$  [70–72], leading to further difference in the plasmon lifetimes of LSCO and LCCO.

## CONCLUSIONS

We have investigated LSCO and LCCO at equal doping using RIXS, and have observed acoustic-like plasmons having different velocities. We find that the plasmon parameters (energy and lifetime) are identical for a given system irrespective of the probed site (Cu or O). While the RIXS cross-section is typically dominated by local-site effects, this observation highlights that the probed charge excitations are non-local and site-independent, similar to magnetic excitations, due to the hybridised nature of valence charge fluctuations. We show that to appropriately describe the acoustic-like plasmon dispersions in cuprates in a mean-field RPA approach one has

to consider renormalized band dispersion parameters. A similar renormalization of the bare band parameters occurs implicitly in the strong-coupling  $t$ - $J$ - $V$  model. This holds true for both sides of the cuprate doping phase diagram, where we observe  $m^*/m > 1$  for both LSCO and LCCO. The comparison with the  $t$ - $J$ - $V$  model, justifies the use of the renormalized band parameters in the RPA approach to effectively represent the mass enhancement stemming from electron correlations at long wavelengths. Therefore, the weak-coupling nature of the RPA should not be used to dismiss its practical usage in cuprates without due consideration. The role of correlations in the two-particle charge response extends beyond a simple adjustment of band parameters. An enhanced band mass reduces the average Fermi velocity and pushes the electron-hole continuum below the plasmon energies, allowing the observation of plasmons as resonant collective excitations. Even though, here we have used an uniform mass enhancement contribution to the acoustic-like plasmon dispersion, optical and ARPES studies on  $\text{Sr}_2\text{RuO}_4$  have suggested the mass enhancement factors to be dependent on the quasiparticle energy [67, 68]. Typically the spin exchange energies ( $\approx 0.2$  eV) are much smaller than the optical plasmon energies of about 1 eV. This may rationalize the non-dependence of optical plasmon dispersion on electron correlations observed using T-EELS in cuprates and ruthenates [30, 54, 73, 74], in contrast to the acoustic plasmons. The difference in the influence of electron correlations on acoustic and optical plasmons will be the subject of our research in the near future.

## IV. METHODS

### A. Experimental details

Single crystal of  $\text{La}_{1.84}\text{Sr}_{0.16}\text{CuO}_4$  (LSCO) grown by floating-zone method and used for previous report on plasmons [31], was reused for this experiment. The crystal was re-cleaved before measurement at each edge, in vacuum. Hole-doping of  $\delta = 0.16$  was verified using magnetisation measurements of LSCO corresponding to superconducting transition temperature of 38 K.

High-quality  $\text{La}_{2-x}\text{Ce}_x\text{CuO}_4$  films were grown on  $\text{SrTiO}_3$  substrates via the pulsed laser deposition technique with 100 nm thickness. The films have a linearly varying Ce concentration ( $x = 0.1$  to 0.19) along the surface of the substrate, fabricated by the continuous moving mask technique [75]. The direction of varying concentration is aligned normal to the RIXS scattering plane. The  $c$ -axis lattice constants and superconducting transition temperatures measured along the concentration gradient direction are consistent with results from single-doping LCCO films [76]. For  $x = 0.16$ , a superconducting transition temperature of 7.87 K was observed using resistivity measurements.

The pressure inside the sample vessel was maintained



around  $5 \times 10^{-10}$  mbar. The samples were cooled down to 25 K. While this means that the LSCO was below and the LCCO was above  $T_C$ , a recent article [14], did not find significant change in the plasmon dispersion in this temperature range. The XAS were collected as total electron yield in normal incidence geometry with  $\sigma$ -polarisation, so that the electric field was in the Cu-O plane. High energy-resolution RIXS spectra were collected at Cu  $L_3$ - ( $\Delta E \simeq 0.045$  eV) and O  $K$ - ( $\Delta E \simeq 0.043$  eV) edges with  $\sigma$ -polarisation, at the I21-RIXS beamline, Diamond Light Source, United Kingdom [77]. The zero-energy transfer position and energy resolution were determined from subsequent measurements of elastic peaks from an adjacent carbon tape. Negative and positive values of  $h$  represent the grazing-incident and grazing-exit geometries, respectively.

RIXS data were normalised to the incident photon flux, and subsequently corrected for self-absorption effects prior to fitting. A Gaussian lineshape with the experimental energy resolution was used to fit the elastic line. Gaussian lineshapes were also used to fit the low energy phonon excitations at  $\sim 0.045$  eV and their overtones. The scattering intensities  $S(\mathbf{q}, \omega)$  of the plasmons, bimagnons and paramagnons, dependent on the imaginary part of their respective dynamic susceptibilities  $\chi''(\mathbf{q}, \omega)$  were modelled as:

$$S(\mathbf{q}, \omega) \propto \frac{\chi''(\mathbf{q}, \omega)}{1 - e^{-\hbar\omega/k_B T}}, \quad (2)$$

where  $k_B$ ,  $T$  and  $\hbar$  are the Boltzmann constant, temperature and the reduced Planck constant. A generic damped harmonic oscillator model was used for the response function

$$\chi''(\mathbf{q}, \omega) \propto \frac{\gamma\omega}{[\omega^2 - \omega_0^2]^2 + 4\omega^2\gamma^2}, \quad (3)$$

where  $\omega_0$  and  $\gamma$  are the undamped frequency and the damping respectively.

First we extracted the zone-centre energy, amplitude and width of the broad incoherent mode at  $h = 0.01$  and concluding this to be a bimagnon, fixed its amplitude and width for the whole momentum-range [31]. The energy values of the bimagnons were allowed to vary within  $\pm 20$  meV. An additional paramagnon component was added for the RIXS spectra at Cu  $L_3$ -edge for LCCO. Significant correlations were found below  $h < 0.02$ , between the elastic, phonon and plasmon amplitudes and energies, and hence the plasmon energy values determined in these regions are less conclusive and not reported. A high energy quadratic background was also included in the fitting model to account for the tailing contribution from  $dd$ -excitations above 1.5 eV. Representative fits using this model are shown in Fig. 2(g-j)

## B. Theory details

### 1. Band dispersion and Coulomb repulsion

Based on *ab-initio* calculations, the electron band dispersion for the cuprates was proposed as:

$$E_{\mathbf{k}} = E_{\mathbf{k}}^{\parallel} + E_{\mathbf{k}}^{\perp}, \quad (4)$$

where the in-plane dispersion  $E_{\mathbf{k}}^{\parallel}$  (Ref. [51]), and the out-of-plane dispersion  $E_{\mathbf{k}}^{\perp}$  are given, respectively, by

$$E_{\mathbf{k}}^{\parallel} = -2t(\cos k_x + \cos k_y) - 4t' \cos k_x \cos k_y - 2t''(\cos 2k_x + \cos 2k_y) - \mu, \quad (5)$$

$$E_{\mathbf{k}}^{\perp} = -\frac{t_z}{4}(\cos k_x - \cos k_y)^2 \cos k_z, \quad (6)$$

with  $\mu$  as the chemical potential. The different hopping pathways in the materials are shown in Fig. 1(a). We use the bare parameters [51]:  $t = 0.4$  eV,  $t'/t = -0.09$ , and  $t''/t = 0.07$  for LSCO, and  $t = 0.4$  eV,  $t'/t = -0.24$ , and  $t''/t = 0.15$  for LCCO. The parameters used for LCCO are those given in Ref. [51] for NCCO, due to unavailability of data for LCCO. In the out-of-plane dispersion  $E_{\mathbf{k}}^{\perp}$  we have neglected  $\cos k_z$  in the calculation, i.e., the contribution of  $E_{\mathbf{k}}^{\perp}$  is independent of  $k_z$  which leads to a non-existing plasmon gap at the zone center, even for a finite value of  $t_z$ . This is justified by the fact that the plasmon gap in LSCO and LCCO, if it exists, is small and at present inaccessible experimentally, a topic which was discussed in depth in Ref. [49]. Therefore, the  $E_{\mathbf{k}}^{\perp}$  dispersion is nearly irrelevant to the present analysis. Thus, without losing generality, we have assumed  $t_z/t = 0.01$  for both systems. We have also neglected  $t'''$  and  $t'_z$ . Finally, we compute the chemical potential  $\mu$  for each case for doping  $\delta = 0.16$ , which gave  $\mu = -0.24$  eV and  $\mu = 0.038$  eV for LSCO and LCCO, respectively.

Earlier works [7, 9, 78], considered the long-range Coulomb interaction  $V(\mathbf{q})$  for homogeneous layered electron gas as

$$V(\mathbf{q}) = V(q_{\parallel}, q_z) = \frac{q_{\parallel} d}{2} \frac{\sinh(q_{\parallel} d)}{\cosh(q_{\parallel} d) - \cos(q_z d)}. \quad (7)$$

Here, we use the long-range Coulomb interaction  $V(\mathbf{q})$  for a layered lattice system for the RPA and  $t$ - $J$ - $V$  models:

$$V(\mathbf{q}) = \frac{V_c}{A(q_x, q_y) - \cos q_z}, \quad (8)$$

where  $V_c = e^2 d (2\epsilon_{\perp} a^2)^{-1}$  and

$$A(q_x, q_y) = \alpha(2 - \cos q_x - \cos q_y) + 1. \quad (9)$$

These expressions are easily obtained by solving the Poisson's equation on the lattice [79]. Here  $\alpha =$

$\tilde{\epsilon}/[(a/d)^2]$ ,  $\tilde{\epsilon} = \epsilon_{\parallel}/\epsilon_{\perp}$ , and  $\epsilon_{\parallel}$  and  $\epsilon_{\perp}$  are the dielectric constants parallel and perpendicular to the planes, respectively. It is important to note that in the present  $V(\mathbf{q})$  model we have two dielectric constants instead of one as in [7, 9].  $e$  is the electric charge of electrons;  $a$  is the in-plane lattice constant and the in-plane momentum  $\mathbf{q}_{\parallel} = (q_x, q_y)$  is calculated in units of  $a^{-1}$ ; similarly  $d$  is the distance between the Cu-O planes, and the out-of-plane momentum  $q_z$  is calculated in units of  $d^{-1}$ . In the present work, we consider  $V_c$  and  $\alpha$  as independent parameters, and from them we can estimate  $\epsilon_{\parallel}$  and  $\epsilon_{\perp}$  and discuss their reliability.

## 2. Random phase approximation

In RPA the charge correlation function is given by the well-known expression [80]

$$\chi_{\text{RPA}}(\mathbf{q}, i\omega_n) = \frac{\chi^{(0)}(\mathbf{q}, i\omega_n)}{1 - V(\mathbf{q})\chi^{(0)}(\mathbf{q}, i\omega_n)}, \quad (10)$$

where  $\chi^{(0)}(\mathbf{q}, i\omega_n)$  is the usual Lindhard function,

$$\chi^{(0)}(\mathbf{q}, i\omega_n) = \frac{2}{N_s} \sum_{\mathbf{k}} \frac{n_F(E_{\mathbf{k}-\mathbf{q}}) - n_F(E_{\mathbf{k}})}{i\omega_n - E_{\mathbf{k}} + E_{\mathbf{k}-\mathbf{q}}}, \quad (11)$$

which accounts for the particle-hole continuum.  $\mathbf{q}$  is a three dimensional wavevector,  $\omega_n$  is a boson Matsubara frequency, and the factor 2 comes from the spin summation.  $N_s$  is the number of sites in each plane and  $n_F$  is the Fermi distribution. The denominator in Eq. 10 is the RPA dielectric function  $\varepsilon(\mathbf{q}, i\omega_n) = 1 - V(\mathbf{q})\chi^{(0)}(\mathbf{q}, i\omega_n)$ .

After performing the analytical continuation  $i\omega_n \rightarrow \omega + i\Gamma$  in  $\chi_{\text{RPA}}(\mathbf{q}, i\omega_n)$ , we obtain the imaginary part of the charge-charge correlation functions  $\chi''_{\text{RPA}}(\mathbf{q}, \omega)$ , which can be directly compared with RIXS. While  $\Gamma (> 0)$  is infinitesimally small, we employ a finite broadening  $\Gamma = 0.04$  eV [28, 32, 81].

The RPA calculation is a weak coupling approach and, in principle, the electron dispersion  $E_{\mathbf{k}}$  (Eq. 4) is given by the bare band [51]. However, as discussed in the text, the electron hopping parameters  $t$ ,  $t'$ , and  $t''$  are renormalized to account for  $m^*/m > 1$ .

The analytical relation between plasmon and Fermi velocities (Eq. 1) in the homogeneous free-electron layered model by Fetter [7] is derived from the plasmon energy:

$$\omega_p = \sqrt{\frac{\langle v_F \rangle^2}{2} q_{\parallel}^2 + \Omega_p^2 \frac{q_{\parallel} d}{2} \frac{\sinh(q_{\parallel} d)}{\cosh(q_{\parallel} d) - \cos(q_{\perp} d)}}, \quad (12)$$

obtained by using the Coulomb potential in Eq. 7 and the denominator in Eq. 10 [7]. Note that in the negligible conduction dissipation limit, the factor  $\langle v_F \rangle^2 q_{\parallel}^2 / 2$  is absent (for  $\omega_p^2 \gg \langle v_F \rangle^2 q_{\parallel}^2 / 2$ ) [82]. This is not the case for the energy-momentum range of plasmons probed in this work.

## 3. The layered $t$ - $J$ - $V$ model and the large- $N$ formalism

The large- $N$  approach for the  $t$ - $J$  model was originally developed in Ref. [83], and extensively used in the context of charge excitations in cuprates, among others, Refs. [27, 28, 31, 49, 81, 84–86]. The aim of this section is to give a brief description of the main formulae.

The layered  $t$ - $J$ - $V$  model is written as

$$H = - \sum_{i,j,\sigma} t_{ij} \tilde{c}_{i\sigma}^{\dagger} \tilde{c}_{j\sigma} + \sum_{\langle i,j \rangle} J_{ij} \left( \vec{S}_i \cdot \vec{S}_j - \frac{1}{4} n_i n_j \right) + \sum_{\langle i,j \rangle} V_{ij} n_i n_j, \quad (13)$$

where the sites  $i$  and  $j$  run over a three-dimensional lattice. The hopping  $t_{ij}$  takes a value  $t$ ,  $t'$  and  $t''$  between the first, second and third nearest-neighbor sites on a square lattice, respectively. The hopping integral between layers is scaled by  $t_z$  (see later for the specific form of the electronic dispersion).  $\langle i, j \rangle$  denotes a nearest-neighbor pair of sites. The exchange interaction  $J_{ij} = J$  is considered only inside the plane; the exchange term between the planes ( $J_{\perp}$ ) is much smaller than  $J$  [87].  $V_{ij}$  is the long-range Coulomb interaction on the lattice and is given in momentum space by Eq. 8.  $\tilde{c}_{i\sigma}^{\dagger}$  ( $\tilde{c}_{i\sigma}$ ) is the creation (annihilation) operator of electrons with spin  $\sigma = (\uparrow, \downarrow)$  in the Fock space without double occupancy.  $n_i = \sum_{\sigma} \tilde{c}_{i\sigma}^{\dagger} \tilde{c}_{i\sigma}$  is the electron density operator and  $\vec{S}_i$  is the spin operator.

In the large- $N$  theory [27] the electronic dispersion  $E_{\mathbf{k}}$  reads:

$$E_{\mathbf{k}} = E_{\mathbf{k}}^{\parallel} + E_{\mathbf{k}}^{\perp}, \quad (14)$$

where

$$E_{\mathbf{k}}^{\parallel} = -2 \left( t \frac{\delta}{2} + \Delta \right) (\cos k_x + \cos k_y) - 4t' \frac{\delta}{2} \cos k_x \cos k_y - 2t'' \frac{\delta}{2} (\cos 2k_x + \cos 2k_y) - \mu, \quad (15)$$

$$E_{\mathbf{k}}^{\perp} = -\frac{t_z \delta}{4} (\cos k_x - \cos k_y)^2 \cos k_z. \quad (16)$$

For a given doping  $\delta$ , the chemical potential  $\mu$  and  $\Delta$  are determined self-consistently by solving

$$\Delta = \frac{J}{4N_s} \sum_{\mathbf{k}} (\cos k_x + \cos k_y) n_F(E_{\mathbf{k}}), \quad (17)$$

and

$$(1 - \delta) = \frac{2}{N_s} \sum_{\mathbf{k}} n_F(E_{\mathbf{k}}). \quad (18)$$

We have obtained for  $\delta = 0.16$  the values  $\mu = -0.044$  eV and  $\Delta = 0.024$  eV for LSCO, and  $\mu = -0.010$  eV and  $\Delta = 0.024$  eV for LCCO.

TABLE II. Parameters extracted by fitting experimental plasmon dispersions to the different models.

	Model	$m^*/m$	$V_c$ (eV)	$\alpha$	$\epsilon_{\parallel}/\epsilon_0$	$\epsilon_{\perp}/\epsilon_0$
LSCO	RPA	1.0	0.49	0.5	14.1	85.1
	RPA	2.0	7.6	3.7	6.72	5.49
	$t$ - $J$ - $V$	-	18.8	4.1	3.01	2.22
LCCO	RPA	1.0	0.9	0.6	10.1	40.8
	RPA	1.7	9.2	3.2	5.05	3.81
	$t$ - $J$ - $V$	-	30.0	3.5	1.71	1.17

In the context of the  $t$ - $J$  model using a path-integral representation [83], for Hubbard operators [88], a six-component bosonic field is defined as

$$\delta X^a = (\delta R, \delta\lambda, r^x, r^y, A^x, A^y), \quad (19)$$

where  $\delta R$  describes fluctuations of the number of holes

at each site, thus, it is related to on-site charge fluctuations,  $\delta\lambda$  is the fluctuation of the Lagrange multiplier introduced to enforce the constraint that prohibits the double occupancy at any site, and  $r^x$  and  $r^y$  ( $A^x$  and  $A^y$ ) describe fluctuations of the real (imaginary) part of the bond field from the  $J$ -term.

The inverse of the  $6 \times 6$  bare bosonic propagator associated with  $\delta X^a$  is

$$\left[ D_{ab}^{(0)}(\mathbf{q}, i\omega_n) \right]^{-1} = N \begin{pmatrix} \frac{\delta^2}{2} [V(\mathbf{q}) - J(\mathbf{q})] & \delta/2 & 0 & 0 & 0 & 0 \\ \delta/2 & 0 & 0 & 0 & 0 & 0 \\ 0 & 0 & \frac{4}{J}\Delta^2 & 0 & 0 & 0 \\ 0 & 0 & 0 & \frac{4}{J}\Delta^2 & 0 & 0 \\ 0 & 0 & 0 & 0 & \frac{4}{J}\Delta^2 & 0 \\ 0 & 0 & 0 & 0 & 0 & \frac{4}{J}\Delta^2 \end{pmatrix}, \quad (20)$$

where  $J(\mathbf{q}) = \frac{J}{2}(\cos q_x + \cos q_y)$ . We use  $J/t = 0.3$ .

At leading order, the bare propagator  $D_{ab}^{(0)}$  is renormalized in  $O(1/N)$ . From the Dyson equation the renormalized bosonic propagator is

$$[D_{ab}(\mathbf{q}, i\omega_n)]^{-1} = [D_{ab}^{(0)}(\mathbf{q}, i\omega_n)]^{-1} - \Pi_{ab}(\mathbf{q}, i\omega_n). \quad (21)$$

Here the  $6 \times 6$  boson self-energy matrix  $\Pi_{ab}$  is

$$\begin{aligned} \Pi_{ab}(\mathbf{q}, i\omega_n) = & -\frac{N}{N_s} \sum_{\mathbf{k}} h_a(\mathbf{k}, \mathbf{q}, E_{\mathbf{k}} - E_{\mathbf{k}-\mathbf{q}}) \\ & \times \frac{n_F(E_{\mathbf{k}-\mathbf{q}}) - n_F(E_{\mathbf{k}})}{i\omega_n - E_{\mathbf{k}} + E_{\mathbf{k}-\mathbf{q}}} h_b(\mathbf{k}, \mathbf{q}, E_{\mathbf{k}} - E_{\mathbf{k}-\mathbf{q}}) \\ & - \delta_{a1}\delta_{b1} \frac{N}{N_s} \sum_{\mathbf{k}} \frac{\tilde{E}_{\mathbf{k}-\mathbf{q}} - \tilde{E}_{\mathbf{k}}}{2} n_F(E_{\mathbf{k}}), \quad (22) \end{aligned}$$

where  $\tilde{E}_{\mathbf{k}}$  is equal to  $E_{\mathbf{k}}$  with  $\Delta = 0$  and the 6-component interaction vertex is given by

$$\begin{aligned} h_a(\mathbf{k}, \mathbf{q}, \nu) = & \left\{ \frac{2E_{\mathbf{k}-\mathbf{q}} + \nu + 2\mu}{2} \right. \\ & + 2\Delta \left[ \cos\left(k_x - \frac{q_x}{2}\right) \cos\left(\frac{q_x}{2}\right) \right. \\ & \left. + \cos\left(k_y - \frac{q_y}{2}\right) \cos\left(\frac{q_y}{2}\right) \right]; 1; \\ & - 2\Delta \cos\left(k_x - \frac{q_x}{2}\right); -2\Delta \cos\left(k_y - \frac{q_y}{2}\right); \\ & \left. 2\Delta \sin\left(k_x - \frac{q_x}{2}\right); 2\Delta \sin\left(k_y - \frac{q_y}{2}\right) \right\}. \quad (23) \end{aligned}$$

In the writing of this manuscript we noted a misprint in the last term of of Eq. 22 in previous works, which has been corrected here.

As discussed previously [83, 84], the element (1, 1) of  $D_{ab}$  is related to the usual charge-charge correlation function  $\chi_{tJV}(\mathbf{r}_i - \mathbf{r}_j, \tau) = \langle T_{\tau} n_i(\tau) n_j(0) \rangle$ , which in the large- $N$  scheme is computed in the  $\mathbf{q}$ - $\omega$  space as

$$\chi_{tJV}(\mathbf{q}, i\omega_n) = N \left( \frac{\delta}{2} \right)^2 D_{11}(\mathbf{q}, i\omega_n). \quad (24)$$

It is important to remark that the charge-charge correlation function is nearly unaffected by the value of  $J$  [71]. As for  $\chi_{\text{RPA}}(\mathbf{q}, i\omega_n)$ , after performing the analytical continuation  $i\omega_n \rightarrow \omega + i\Gamma$  in  $\chi_{tJV}(\mathbf{q}, i\omega_n)$  we obtain the

imaginary part of the charge-charge correlation functions  $\chi''_{tJV}(\mathbf{q}, \omega)$ . The plasmon excitations are obtained for the resonant peaks of  $\chi''_{tJV}(\mathbf{q}, \omega)$ .

#### 4. Correlations in the $t$ - $J$ - $V$ and RPA models

Here, we discuss the effects of correlations on the plasmon dispersion which can and cannot be captured using RPA with an enhancement in  $m^*/m$  by comparing with the  $t$ - $J$ - $V$  model. The large- $N$  formalism within the  $t$ - $J$ - $V$  model renormalizes the band parameters due to electron correlations, which can be seen in the band dispersion directly (Eqs. 14-16). Comparing it to the usual tight-binding dispersion (Eqs. 4-6), we obtain

$$\begin{aligned} t_{\text{eff}} &= t\delta + \Delta, \\ t'_{\text{eff}} &= t'\delta, \\ t''_{\text{eff}} &= t''\delta, \\ t_{z\text{eff}} &= t_z\delta, \end{aligned} \quad (25)$$

where the hopping parameters  $t$ ,  $t'$ ,  $t''$ , and  $t_z$  are the tight-binding bare ones. We introduced these effective parameters into the RPA model and plotted the obtained plasmon dispersion in Fig. 5. To understand the deviation at large-momenta between RPA and  $t$ - $J$ - $V$ , we consider only the  $2 \times 2$  sector ( $a, b = 1, 2$ ) in the  $D_{ab}(\mathbf{q}, i\omega_n)$  (Eq 21). If in Eq 21 we set manually the bosonic self-energy components  $\Pi_{11}$  and  $\Pi_{12}$  to zero, the only relevant component is  $\Pi_{22}$ , and from Eqs. 22 and 23 it can be written as

$$\begin{aligned} \Pi_{22}(\mathbf{q}, i\omega_n) &= -N \sum_{\mathbf{k}} \frac{n_F(E_{\mathbf{k}-\mathbf{q}}) - n_F(E_{\mathbf{k}})}{i\omega_n - E_{\mathbf{k}} + E_{\mathbf{k}-\mathbf{q}}} \\ &= -N \frac{\chi_0(\mathbf{q}, i\omega_n)}{2}. \end{aligned} \quad (26)$$

In spite of  $\chi_0$  (Eq. 11) representing the particle-hole continuum within the RPA and  $\Pi_{22}$  appearing in the large- $N$

formalism within the  $t$ - $J$ - $V$  model as only one component of the bosonic self-energy carrying the information of the fluctuations of the Lagrange multiplier associated with the constraint that prohibits the double occupancy, both have a similar mathematical form. In this context, we compute  $\chi_{tJV}(\mathbf{q}, i\omega_n)$  in Eq. 24 using the physical value  $N = 2$  [27] which gives

$$\chi_{tJV}(\mathbf{q}, i\omega_n) = \frac{\chi_0(\mathbf{q}, i\omega_n)}{1 - V'(\mathbf{q})\chi_0(\mathbf{q}, i\omega_n)}. \quad (27)$$

where  $V'(\mathbf{q}) = 2[V(\mathbf{q}) - J(\mathbf{q})]$ . Eq. 27 shows that the charge-charge correlation function in the large- $N$  formalism considering only the contribution from  $\Pi_{22}$  has an RPA-like mathematical form. This shows the presence of a "hidden" RPA structure with electronic correlations within the  $t$ - $J$ - $V$  formalism with respect to RPA. The contribution of  $J(\mathbf{q})$  can be neglected because  $V(\mathbf{q})$  is significantly larger, and the factor 2 accounts for the transformation to eV using the renormalized value of  $t$  in the large- $N$  formalism.

#### ACKNOWLEDGMENTS

We thank A. A. Aligia, M. Hepting, C. Falter and W. S. Lee for discussions and comments. A part of the results presented in this work was obtained by using the facilities of the CCT-Rosario Computational Center, member of the High Performance Computing National System (SNCAD, MincyT-Argentina). J.C. acknowledges financial support from the National Research Foundation of Korea (NRF) funded by the Korean government (MSIT) through Sejong Science Fellowship (Grant No. RS-2023-00252768). Z.L. acknowledges the National Natural Science Foundation of China (12225412), and CAS Project for Young Scientists in Basic Research (2022YSBR-048). H.Y. was supported by JSPS KAKENHI Grant No. JP20H01856 and World Premier International Research Center Initiative (WPI), MEXT, Japan.

- 
- [1] C. Proust and L. Taillefer, The remarkable underlying ground states of cuprate superconductors, *Annu. Rev. Condens. Matter Phys.* **10**, 409 (2019).
  - [2] B. Keimer, S. A. Kivelson, M. R. Norman, S. Uchida, and J. Zaanen, From quantum matter to high-temperature superconductivity in copper oxides, *Nature* **518**, 179 (2015).
  - [3] A. Kaiser, A. Snezhko, and I. S. Aranson, Flocking ferromagnetic colloids, *Science Advances* **3**, e1601469 (2017).
  - [4] D. R. Chialvo, Emergent complex neural dynamics, *Nat. Phys.* **6**, 744 (2010).
  - [5] D. Pines and D. Bohm, A collective description of electron interactions: II. Collective vs. individual particle aspects of the interactions, *Physical Review* **85**, 338 (1952).
  - [6] I. Bozovic, Plasmons in cuprate superconductors, *Phys. Rev. B* **42**, 1969 (1990).
  - [7] A. L. Fetter, Electrodynamics of a layered electron gas. II. Periodic array, *Ann. Phys.* **88**, 1 (1974).
  - [8] R. S. Markiewicz, M. Z. Hasan, and A. Bansil, Acoustic plasmons and doping evolution of Mott physics in resonant inelastic x-ray scattering from cuprate superconductors, *Phys. Rev. B* **77**, 094518 (2008).
  - [9] D. Grecu, Plasma frequency of the electron gas in layered structures, *Phys. Rev. B* **8**, 1958 (1973).
  - [10] N. Nücker, H. Romberg, S. Nakai, B. Scheerer, J. Fink, Y. F. Yan, and Z. X. Zhao, Plasmons and interband transitions in  $\text{Bi}_2\text{Sr}_2\text{CaCu}_2\text{O}_8$ , *Phys. Rev. B* **39**, 12379(R) (1989).
  - [11] M. Hepting, L. Chaix, E. W. Huang, R. Fumagalli, Y. Y. Peng, B. Moritz, K. Kummer, N. B. Brookes, W. C. Lee, M. Hashimoto, T. Sarkar, J.-F. He, C. R. Rotundu, Y. S. Lee, R. L. Greene, L. Braicovich, G. Ghiringhelli, Z. X.



- Shen, T. P. Devereaux, and W. S. Lee, Three-dimensional collective charge excitations in electron-doped copper oxide superconductors, *Nature* **563**, 374 (2018).
- [12] J. Lin, J. Yuan, K. Jin, Z. Yin, G. Li, K.-J. Zhou, X. Lu, M. Dantz, T. Schmitt, H. Ding, H. Guo, M. P. M. Dean, and X. Liu, Doping evolution of the charge excitations and electron correlations in electron-doped superconducting  $\text{La}_{2-x}\text{Ce}_x\text{CuO}_4$ , *npj Quantum Mater.* **5**, 4 (2020).
- [13] A. Singh, H. Y. Huang, C. Lane, J. H. Li, J. Okamoto, S. Komiya, R. S. Markiewicz, A. Bansil, A. Fujimori, C. T. Chen, and D. J. Huang, Acoustic plasmons and conducting carriers in hole-doped cuprate superconductors, *Phys. Rev. B* **105**, 235105 (2022).
- [14] M. Hepting, T. D. Boyko, V. Zimmermann, M. Bejas, Y. E. Suyolcu, P. Puphal, R. J. Green, L. Zinni, J. Kim, D. Casa, M. H. Upton, D. Wong, C. Schulz, M. Bartkowiak, K. Habicht, E. Pomjakushina, G. Cristiani, G. Logvenov, M. Minola, H. Yamase, A. Greco, and B. Keimer, Evolution of plasmon excitations across the phase diagram of the cuprate superconductor  $\text{La}_{2-x}\text{Sr}_x\text{CuO}_4$ , *Phys. Rev. B* **107**, 214516 (2023).
- [15] Q. Li, L. Ju, H. Huang, Y. Zhang, C. Zou, T. Ren, A. Singh, S. Zhang, Q. Qiu, Q. Xiao, D.-J. Huang, Y. Xie, Z. Chen, and Y. Peng, *Charge redistribution, charge order and plasmon in  $\text{La}_{2-x}\text{Sr}_x\text{CuO}_4/\text{La}_2\text{CuO}_4$  superlattices* (2023), arXiv:2309.01649 [cond-mat].
- [16] M. Bejas, V. Zimmermann, D. Betto, T. D. Boyko, R. J. Green, T. Loew, N. B. Brookes, G. Cristiani, G. Logvenov, M. Minola, B. Keimer, H. Yamase, A. Greco, and M. Hepting, Plasmon dispersion in bilayer cuprate superconductors, *Phys. Rev. B* **109**, 144516 (2024).
- [17] V. Z. Kresin and H. Morawitz, Layer plasmons and high- $T_c$  superconductivity, *Phys. Rev. B* **37**, 7854 (1988).
- [18] J. Levallois, M. Tran, D. Pouliot, C. Presura, L. Greene, J. Eckstein, J. Uccelli, E. Giannini, G. Gu, A. Leggett, and D. van der Marel, Temperature-dependent ellipsometry measurements of partial coulomb energy in superconducting cuprates, *Phys. Rev. X* **6**, 031027 (2016).
- [19] A. Bill, H. Morawitz, and V. Z. Kresin, Electronic collective modes and superconductivity in layered conductors, *Phys. Rev. B* **68**, 144519 (2003).
- [20] T. Bauer and C. Falter, Impact of dynamical screening on the phonon dynamics of metallic  $\text{La}_2\text{CuO}_4$ , *Phys. Rev. B* **80**, 094525 (2009).
- [21] C. Falter and M. Klenner, Nonadiabatic and nonlocal electron-phonon interaction and phonon-plasmon mixing in the high-temperature superconductors, *Phys. Rev. B* **50**, 9426 (1994).
- [22] G. Dellea, M. Minola, A. Galdi, D. Di Castro, C. Aruta, N. B. Brookes, C. J. Jia, C. Mazzoli, M. Moretti Sala, B. Moritz, P. Orgiani, D. G. Schlom, A. Tebano, G. Balestrino, L. Braicovich, T. P. Devereaux, L. Maritato, and G. Ghiringhelli, Spin and charge excitations in artificial hole- and electron-doped infinite layer cuprate superconductors, *Phys. Rev. B* **96**, 115117 (2017).
- [23] D. Meyers, H. Miao, A. C. Walters, V. Bisogni, R. S. Springell, M. d'Astuto, M. Dantz, J. Pelliciani, H. Y. Huang, J. Okamoto, D. J. Huang, J. P. Hill, X. He, I. Božović, T. Schmitt, and M. P. M. Dean, Doping dependence of the magnetic excitations in  $\text{La}_{2-x}\text{Sr}_x\text{CuO}_4$ , *Phys. Rev. B* **95**, 075139 (2017).
- [24] H. C. Robarts, M. Barthélemy, K. Kummer, M. García-Fernández, J. Li, A. Nag, A. C. Walters, K. J. Zhou, and S. M. Hayden, Anisotropic damping and wave vector dependent susceptibility of the spin fluctuations in  $\text{La}_{2-x}\text{Sr}_x\text{CuO}_4$  studied by resonant inelastic x-ray scattering, *Phys. Rev. B* **100**, 214510 (2019).
- [25] J. Spałek, M. Fidrysiak, M. Zegrodnik, and A. Biborski, Superconductivity in high- $T_c$  and related strongly correlated systems from variational perspective: Beyond mean field theory, *Phys. Rep.* **959**, 1 (2022).
- [26] M. Fidrysiak and J. Spałek, A unified theory of spin and charge excitations in high- $T_c$  cuprates: Quantitative comparison with experiment and interpretation, *Phys. Rev. B* **104**, L020510 (2021).
- [27] A. Greco, H. Yamase, and M. Bejas, Plasmon excitations in layered high- $T_c$  cuprates, *Phys. Rev. B* **94**, 075139 (2016).
- [28] A. Greco, H. Yamase, and M. Bejas, Origin of high-energy charge excitations observed by resonant inelastic X-ray scattering in cuprate superconductors, *Commun. Phys.* **2**, 3 (2019).
- [29] R. Comin and A. Damascelli, ARPES: A Probe of Electronic Correlations, in *Strongly Correlated Systems: Experimental Techniques*, edited by A. Avella and F. Mancini (Springer, Berlin, Heidelberg, 2015) pp. 31–71.
- [30] N. Nücker, U. Eckern, J. Fink, and P. Müller, Long-wavelength collective excitations of charge carriers in high- $T_c$  superconductors, *Phys. Rev. B* **44**, 7155 (1991).
- [31] A. Nag, M. Zhu, M. Bejas, J. Li, H. C. Robarts, H. Yamase, A. N. Petsch, D. Song, H. Eisaki, A. C. Walters, M. García-Fernández, A. Greco, S. M. Hayden, and K.-J. Zhou, Detection of acoustic plasmons in hole-doped lanthanum and bismuth cuprate superconductors using resonant inelastic x-ray scattering, *Phys. Rev. Lett.* **125**, 257002 (2020).
- [32] P. Prelovšek and P. Horsch, Electron-energy loss spectra and plasmon resonance in cuprates, *Phys. Rev. B* **60**, R3735 (1999).
- [33] M. Mitrano, A. A. Husain, S. Vig, A. Kogar, M. S. Rak, S. I. Rubeck, J. Schmalian, B. Uchoa, J. Schneeloch, R. Zhong, G. D. Gu, and P. Abbamonte, Anomalous density fluctuations in a strange metal, *Proc. Natl. Acad. Sci. U.S.A.* **115**, 5392 (2018).
- [34] A. A. Husain, M. Mitrano, M. S. Rak, S. I. Rubeck, B. Uchoa, J. Schneeloch, R. Zhong, G. D. Gu, and P. Abbamonte, Crossover of charge fluctuations across the strange metal phase diagram, *Phys. Rev. X* **9**, 041062 (2019).
- [35] A. Romero-Bermúdez, A. Krikun, K. Schalm, and J. Zaanen, Anomalous attenuation of plasmons in strange metals and holography, *Phys. Rev. B* **99**, 235149 (2019).
- [36] B. Moritz, F. Schmitt, W. Meevasana, S. Johnston, E. M. Motoyama, M. Greven, D. H. Lu, C. Kim, R. T. Scalettar, Z.-X. Shen, and T. P. Devereaux, Effect of strong correlations on the high energy anomaly in hole- and electron-doped high- $T_c$  superconductors, *New J. Phys.* **11**, 093020 (2009).
- [37] H. Das and T. Saha-Dasgupta, Electronic structure of  $\text{La}_2\text{CuO}_4$  in the  $T$  and  $T'$  crystal structures using dynamical mean field theory, *Phys. Rev. B* **79**, 134522 (2009).
- [38] C. Weber, K. Haule, and G. Kotliar, Apical oxygens and correlation strength in electron- and hole-doped copper

- oxides, *Phys. Rev. B* **82**, 125107 (2010).
- [39] P. A. Lee, N. Nagaosa, and X.-G. Wen, Doping a Mott insulator: Physics of high-temperature superconductivity, *Rev. Mod. Phys.* **78**, 17 (2006).
- [40] J. Zaanen, G. A. Sawatzky, and J. W. Allen, Band gaps and electronic structure of transition-metal compounds, *Phys. Rev. Lett.* **55**, 418 (1985).
- [41] V. J. Emery, Theory of high- $T_c$  superconductivity in oxides, *Phys. Rev. Lett.* **58**, 2794 (1987).
- [42] C. Varma, S. Schmitt-Rink, and E. Abrahams, Charge transfer excitations and superconductivity in “ionic” metals, *Solid State Commun.* **62**, 681 (1987).
- [43] C. T. Chen, F. Sette, Y. Ma, M. S. Hybertsen, E. B. Stechel, W. M. C. Foulkes, M. Schuller, S.-W. Cheong, A. S. Cooper, L. W. Rupp, B. Batlogg, Y. L. Soo, Z. H. Ming, A. Krol, and Y. H. Kao, Electronic states in  $\text{La}_{2-x}\text{Sr}_x\text{CuO}_{4+\delta}$  probed by soft-x-ray absorption, *Phys. Rev. Lett.* **66**, 104 (1991).
- [44] N. P. Armitage, P. Fournier, and R. L. Greene, Progress and perspectives on electron-doped cuprates, *Rev. Mod. Phys.* **82**, 2421 (2010).
- [45] J. Fink, N. Nücker, E. Pellegrin, H. Romberg, M. Alexander, and M. Knupfer, Electron energy-loss and x-ray absorption spectroscopy of cuprate superconductors and related compounds, *J. Electron. Spectrosc. Relat. Phenom.* **66**, 395 (1994).
- [46] E. Pellegrin, N. Nücker, J. Fink, S. L. Molodtsov, A. Gutiérrez, E. Navas, O. Strebler, Z. Hu, M. Domke, G. Kaindl, S. Uchida, Y. Nakamura, J. Markl, M. Klauda, G. Saemann-Ischenko, A. Krol, J. L. Peng, Z. Y. Li, and R. L. Greene, Orbital character of states at the Fermi level in  $\text{La}_{2-x}\text{Sr}_x\text{CuO}_4$  and  $\text{R}_{2-x}\text{Ce}_x\text{CuO}_4$  ( $R=\text{Nd, Sm}$ ), *Phys. Rev. B* **47**, 3354 (1993).
- [47] H. Miao, J. Lorenzana, G. Seibold, Y. Y. Peng, A. Amorese, F. Yakhou-Harris, K. Kummer, N. B. Brookes, R. M. Konik, V. Thampy, G. D. Gu, G. Ghiringhelli, L. Braicovich, and M. P. M. Dean, High-temperature charge density wave correlations in  $\text{La}_{1.875}\text{Ba}_{0.125}\text{CuO}_4$  without spin-charge locking, *Proc. Natl. Acad. Sci. U.S.A.* **114**, 12430 (2017).
- [48] W. S. Lee, J. J. Lee, E. A. Nowadnick, S. Gerber, W. Tabis, S. W. Huang, V. N. Strocov, E. M. Motoyama, G. Yu, B. Moritz, H. Y. Huang, R. P. Wang, Y. B. Huang, W. B. Wu, C. T. Chen, D. J. Huang, M. Greven, T. Schmitt, Z. X. Shen, and T. P. Devereaux, Asymmetry of collective excitations in electron- and hole-doped cuprate superconductors, *Nat. Phys.* **10**, 883 (2014).
- [49] M. Hepting, M. Bejas, A. Nag, H. Yamase, N. Coppola, D. Betto, C. Falter, M. Garcia-Fernandez, S. Agrestini, K.-J. Zhou, M. Minola, C. Sacco, L. Maritato, P. Orgiani, H. Wei, K. Shen, D. Schlom, A. Galdi, A. Greco, and B. Keimer, Gapped collective charge excitations and interlayer hopping in cuprate superconductors, *Phys. Rev. Lett.* **129**, 047001 (2022).
- [50] S. Uchida, T. Ido, H. Takagi, T. Arima, Y. Tokura, and S. Tajima, Optical spectra of  $\text{La}_{2-x}\text{Sr}_x\text{CuO}_4$ : Effect of carrier doping on the electronic structure of the  $\text{CuO}_2$  plane, *Phys. Rev. B* **43**, 7942 (1991).
- [51] R. S. Markiewicz, S. Sahrakorpi, M. Lindroos, H. Lin, and A. Bansil, One-band tight-binding model parametrization of the high- $T_c$  cuprates including the effect of  $k_z$  dispersion, *Phys. Rev. B* **72**, 054519 (2005).
- [52] J. Fink, M. Knupfer, S. Atzkern, and M. Golden, Electronic correlations in solids, studied using electron energy-loss spectroscopy, *J. Electron. Spectrosc. Relat. Phenom.* **117-118**, 287 (2001).
- [53] V. G. Grigoryan, G. Paasch, and S.-L. Drechsler, Determination of an effective one-electron spectrum from the plasmon dispersion of nearly optimally doped  $\text{Bi}_2\text{Sr}_2\text{CaCu}_2\text{O}_8$ , *Phys. Rev. B* **60**, 1340 (1999).
- [54] J. Schultz, A. Lubk, F. Jerzembeck, N. Kikugawa, M. Knupfer, D. Wolf, B. Büchner, and J. Fink, Optical and acoustic plasmons in the layered material  $\text{Sr}_2\text{RuO}_4$  (2024), arXiv:2401.05880 [cond-mat].
- [55] A. A. Husain, E. W. Huang, M. Mitrano, M. S. Rak, S. I. Rubeck, X. Guo, H. Yang, C. Sow, Y. Maeno, B. Uchoa, T. C. Chiang, P. E. Batson, P. W. Phillips, and P. Abbamonte, Pines’ demon observed as a 3D acoustic plasmon in  $\text{Sr}_2\text{RuO}_4$ , *Nature* **621**, 66 (2023).
- [56] A. Ino, C. Kim, M. Nakamura, T. Yoshida, T. Mizokawa, A. Fujimori, Z.-X. Shen, T. Kakeshita, H. Eisaki, and S. Uchida, Doping-dependent evolution of the electronic structure of  $\text{La}_{2-x}\text{Sr}_x\text{CuO}_4$  in the superconducting and metallic phases, *Phys. Rev. B* **65**, 094504 (2002).
- [57] C. Weber, K. Haule, and G. Kotliar, Strength of correlations in electron- and hole-doped cuprates, *Nat. Phys.* **6**, 574 (2010).
- [58] A. Kobayashi, A. Tsuruta, T. Matsuura, and Y. Kuroda, The electron-hole asymmetry in the cuprate superconductors, *Physica C* **388-389**, 39 (2003).
- [59] K. Segawa, M. Kofu, S.-H. Lee, I. Tsukada, H. Hiraka, M. Fujita, S. Chang, K. Yamada, and Y. Ando, Zero-doping state and electron-hole asymmetry in an ambipolar cuprate, *Nat. Phys.* **6**, 579 (2010).
- [60] R. Mizuno, M. Ochi, and K. Kuroki, DMFT study on the electron-hole asymmetry of the electron correlation strength in the high  $T_c$  cuprates, *J. Phys. Soc. Jpn.* **86**, 114706 (2017).
- [61] D. Ogura and K. Kuroki, Asymmetry of superconductivity in hole- and electron-doped cuprates: Explanation within two-particle self-consistent analysis for the three-band model, *Phys. Rev. B* **92**, 144511 (2015).
- [62] L. de’ Medici, X. Wang, M. Capone, and A. J. Millis, Correlation strength, gaps, and particle-hole asymmetry in high- $T_c$  cuprates: A dynamical mean field study of the three-band copper-oxide model, *Phys. Rev. B* **80**, 054501 (2009).
- [63] G. Paasch, Influence of interband transitions on plasmons in the alkali metals; pseudopotential calculation, *Phys. Status Solidi B* **38**, A123 (1970).
- [64] P. C. Gibbons and S. E. Schnatterly, Comment on the line shape of the plasma resonance in simple metals, *Phys. Rev. B* **15**, 2420 (1977).
- [65] A. vom Felde, J. Sprösser-Prou, and J. Fink, Valence-electron excitations in the alkali metals, *Phys. Rev. B* **40**, 10181 (1989).
- [66] H. Hafermann, E. G. C. P. van Loon, M. I. Katsnelson, A. I. Lichtenstein, and O. Parcollet, Collective charge excitations of strongly correlated electrons, vertex corrections, and gauge invariance, *Phys. Rev. B* **90**, 235105 (2014).
- [67] D. Stricker, J. Mravlje, C. Berthod, R. Fittipaldi, A. Vecchione, A. Georges, and D. van der Marel, Optical response of  $\text{Sr}_2\text{RuO}_4$  reveals universal fermi-liquid scaling and quasiparticles beyond landau theory, *Phys. Rev. Lett.* **113**, 087404 (2014).
- [68] A. Hunter, S. Beck, E. Cappelli, F. Margot, M. Straub, Y. Alexanian, G. Gatti, M. Watson, T. Kim, C. Cacho,

- N. Plumb, M. Shi, M. Radović, D. Sokolov, A. Mackenzie, M. Zingl, J. Mravlje, A. Georges, F. Baumberger, and A. Tamai, Fate of quasiparticles at high temperature in the correlated metal  $\text{Sr}_2\text{RuO}_4$ , *Phys. Rev. Lett.* **131**, 236502 (2023).
- [69] B. Michon, C. Berthod, C. W. Rischau, A. Ataei, L. Chen, S. Komiya, S. Ono, L. Taillefer, D. van der Marel, and A. Georges, Reconciling scaling of the optical conductivity of cuprate superconductors with Planckian resistivity and specific heat, *Nat. Commun.* **14**, 3033 (2023).
- [70] G. Khaliullin and P. Horsch, Theory of the density fluctuation spectrum of strongly correlated electrons, *Phys. Rev. B* **54**, R9600 (1996).
- [71] M. Bejas, H. Yamase, and A. Greco, Dual structure in the charge excitation spectrum of electron-doped cuprates, *Phys. Rev. B* **96**, 214513 (2017).
- [72] M. Zafur and H. Yamase, Spin and bond-charge excitation spectra in correlated electron systems near an antiferromagnetic phase, *Phys. Rev. B* **109**, 245127 (2024).
- [73] M. Knupfer, F. Jerzembeck, N. Kikugawa, F. Roth, and J. Fink, Propagating charge carrier plasmon in  $\text{Sr}_2\text{RuO}_4$ , *Phys. Rev. B* **106**, L241103 (2022).
- [74] F. Roth, A. Revcolevschi, B. Büchner, M. Knupfer, and J. Fink, Evidence for an orbital dependent Mott transition in the ladders of  $(\text{La,Ca})_x\text{Sr}_{14-x}\text{Cu}_{24}\text{O}_{41}$  derived by electron energy loss spectroscopy, *Phys. Rev. B* **101**, 195132 (2020).
- [75] J. Yuan, Q. Chen, K. Jiang, Z. Feng, Z. Lin, H. Yu, G. He, J. Zhang, X. Jiang, X. Zhang, Y. Shi, Y. Zhang, M. Qin, Z. G. Cheng, N. Tamura, Y.-f. Yang, T. Xiang, J. Hu, I. Takeuchi, K. Jin, and Z. Zhao, Scaling of the strange-metal scattering in unconventional superconductors, *Nature* **602**, 431 (2022).
- [76] A. Sawa, M. Kawasaki, H. Takagi, and Y. Tokura, Electron-doped superconductor  $\text{La}_{2-x}\text{Ce}_x\text{CuO}_4$ : Preparation of thin films and modified doping range for superconductivity, *Phys. Rev. B* **66**, 014531 (2002).
- [77] K.-J. Zhou, A. Walters, M. Garcia-Fernandez, T. Rice, M. Hand, A. Nag, J. Li, S. Agrestini, P. Garland, H. Wang, S. Alcock, I. Nistea, B. Nutter, N. Rubies, G. Knap, M. Gaughran, F. Yuan, P. Chang, J. Emmins, and G. Howell, I21: an advanced high-resolution resonant inelastic X-ray scattering beamline at Diamond Light Source, *J. Synchrotron Radiat.* **29**, 563 (2022).
- [78] A. L. Fetter, Electrostatics of a layered electron gas. I. Single layer, *Ann. Phys.* **81**, 367 (1973).
- [79] F. Becca, M. Tarquini, M. Grilli, and C. Di Castro, Charge-density waves and superconductivity as an alternative to phase separation in the infinite-U Hubbard-Holstein model, *Phys. Rev. B* **54**, 12443 (1996).
- [80] G. D. Mahan, *Many-Particle Physics* (Springer US, Boston, MA, 1990).
- [81] A. Greco, H. Yamase, and M. Bejas, Close inspection of plasmon excitations in cuprate superconductors, *Phys. Rev. B* **102**, 024509 (2020).
- [82] A. A. Zabolotnykh and V. A. Volkov, Plasmons and magnetoplasmons in partially bounded two-layer electron systems, *Phys. Rev. B* **102**, 165306 (2020).
- [83] A. Foussats and A. Greco, Large- $N$  expansion based on the Hubbard operator path integral representation and its application to the  $t$ - $J$  model. II. The case for finite  $J$ , *Phys. Rev. B* **70**, 205123 (2004).
- [84] M. Bejas, A. Greco, and H. Yamase, Possible charge instabilities in two-dimensional doped Mott insulators, *Phys. Rev. B* **86**, 224509 (2012).
- [85] H. Yamase, M. Bejas, and A. Greco, Electron self-energy from quantum charge fluctuations in the layered  $t$ - $J$  model with long-range Coulomb interaction, *Phys. Rev. B* **104**, 045141 (2021).
- [86] H. Yamase, M. Bejas, and A. Greco, Plasmarons in high-temperature cuprate superconductors, *Commun. Phys.* **6**, 1 (2023).
- [87] T. Thio, T. R. Thurston, N. W. Preyer, P. J. Picone, M. A. Kastner, H. P. Jenssen, D. R. Gabbe, C. Y. Chen, R. J. Birgeneau, and A. Aharony, Antisymmetric exchange and its influence on the magnetic structure and conductivity of  $\text{La}_2\text{CuO}_4$ , *Phys. Rev. B* **38**, 905 (1988).
- [88] J. Hubbard, Electron correlations in narrow energy bands, *Proc. R. Soc. London, Ser. A* **276**, 238 (1963).